Eur. J. Mineral.
2019, **31**, 973–982
Published online 29 July 2019

Alabandite (MnS) in metamorphosed manganiferous rocks at Morro da Mina, Brazil: palaeoenvironmental significance

Alexandre Raphael CABRAL[1,2,*], Armin ZEH[3], Nívea Cristina da Silva VIANA[4], Marco Paulo DE CASTRO[5], František LAUFEK[6], Bernd LEHMANN[7] and Gláucia QUEIROGA[5]

[1]Centro de Pesquisas Professor Manoel Teixeira da Costa (CPMTC), Instituto de Geociências, Universidade Federal de Minas Gerais (UFMG), Av. Antônio Carlos 6.627, 31270-901 Belo Horizonte, Minas Gerais, Brazil
*Corresponding author, e-mail: arcab@ufmg.br
[2]Centro de Desenvolvimento da Tecnologia Nuclear (CDTN), Av. Antônio Carlos 6.627, 31270-901 Belo Horizonte, Minas Gerais, Brazil
[3]Institut für Angewandte Geowissenschaften – Mineralogie und Petrologie, Karlsruher Institut für Technologie (KIT), Adenauerring 20b, Geb. 50.40, 76131 Karlsruhe, Germany
[4]Vale Manganês S.A., Rua Duque de Caxias s/n, Morro da Mina, 36400-000 Conselheiro Lafaiete, Minas Gerais, Brazil
[5]Departamento de Geologia, Escola de Minas, Universidade Federal de Ouro Preto, Morro do Cruzeiro, 35400-000 Ouro Preto, Minas Gerais, Brazil
[6]Czech Geological Survey, Geologická 6, 152 00 Praha 5, Czech Republic
[7]Mineral Resources, Technische Universität Clausthal, Adolph-Roemer-Str. 2a, 38678 Clausthal-Zellerfeld, Germany

Abstract: The mineral alabandite, cubic MnS with variable amounts of FeS, occurs in a number of mineral assemblages in manganiferous metasedimentary rocks, some of which are mined as manganese ore. One of them is Morro da Mina, Mina Gerais, Brazil, where alabandite is a minor component of "queluzite", a manganese-silicate–carbonate rock. The Morro da Mina alabandite contains 7.3 ± 1.4 mol% FeS and makes up aggregates with graphite and molybdenite. A comparison of alabandite occurrences worldwide indicates four main types of mineral assemblages: (1) alabandite + graphite; (2) alabandite + graphite + molybdenite; (3) alabandite + rhodochrosite + molybdenite; (4) and alabandite + rhodochrosite. The different assemblages suggest that manganese sulfide formed in a range of marine palaeoenvironments, from highly reducing and sulfidic – *i.e.*, euxinic – settings to manganese-oxide-precipitating conditions. Morro da Mina represents assemblage (2), which is characteristic of a euxinic water column in a stratified ocean. In general, our comparison of alabandite-bearing mineral assemblages indicates that palaeoenvironmental information can be retrieved from sedimentary rocks that experienced variable degrees of metamorphic overprint.

Key-words: alabandite; graphite; molybdenite; palaeoenvironment; redox conditions; manganese ore.

1. Introduction

Authigenic manganese sulfide, MnS, is thought to develop in sediments undergoing extensive organic-matter decomposition (Baron & Debyser, 1957; Suess, 1979; Böttcher & Huckriede, 1997). In addition to hexagonal MnS, the cubic variety, known as the mineral alabandite, occurs in anoxic sediments where H_2S exceeded iron availability (Lepland & Stevens, 1998). Its formation requires very high activities of H_2S, which can only be achieved in extreme euxinic – *i.e.*, sulfidic – sedimentary environments. Such extreme environments are, however, uncommon (*e.g.*, Berner, 1981), and regarded as unexpected in most sedimentary-diagenetic environments (Roy, 1992). Thus, the finding of MnS in carbon-rich sedimentary rocks and their metamorphic counterparts has a great potential to constrain the palaeoenvironmental conditions at the time of sediment deposition.

Alabandite was reported by Part *et al.* (1951) as a rock-forming mineral of the so-called silicate–carbonate protore of the Morro da Mina manganese-ore deposit, Minas Gerais (Brazil). At that time, the Morro da Mina manganese ore consisted of manganese-oxide minerals that originated from the weathering of a manganese-silicate–carbonate rock, or protore. Currently, the manganese ore mined at Morro da Mina is the manganese-silicate–carbonate rock itself, known as "queluzite". This rock, initially defined by Derby (1901, 1908), contains manganese carbonate as a key component (Roy, 1965), together with ubiquitous graphite and a variety of manganese-silicate minerals, such as spessartine, rhodonite, pyroxmangite and tephroite (Hussak, 1906; Miller & Singewald, 1917; Guimarães, 1929; Candia & Girardi, 1979; Pires, 1983; Viana, 2009). The term queluzite has been used to describe manganese-silicate–carbonate ores worldwide (Roy & Purkait, 1968; Jinglan, 1987; Dasgupta *et al.*, 1990; Gutzmer & Beukes, 2009).

https://doi.org/10.1127/ejm/2019/0031-2879 0935-1221/19/0031-2879 $ 4.50

Since its record in the camera-lucida sketch of Park *et al.* (1951), the Morro da Mina alabandite has lacked proper documentation and characterisation. Its chemical composition has not been assessed. Here, we document the occurrence of alabandite at Morro da Mina, characterising its chemical composition by electron-microprobe analysis. Furthermore, we compare our electron-microprobe results with those available for alabandite from other metasedimentary settings, followed by a discussion on alabandite in metasedimentary rocks as a palaeoenvironmental indicator.

2. Geological setting and manganese mineralisation

Morro da Mina has been mined for manganese since 1902. The deposit is situated to the south of the Quadrilátero Ferrífero of Minas Gerais, about 35 km southwest of Ouro Preto (Fig. 1). The main ore type at Morro da Mina is queluzite. This manganese-silicate–carbonate rock is characteristic of the Lafaiete Formation, which is traceable for over 100 km in the Barbacena greenstone belt (Ebert, 1957, 1962; Pires, 1978). The greenstone belt and its manganese-rich unit have been considered Archaean in age (*e.g.*, Grossi Sad *et al.*, 1983; Noce *et al.*, 2000). However, the deposition of the manganese-rich sediments that gave rise to the Morro da Mina queluzite can be constrained between 2.07 and 1.86 Ga, as indicated by U–Pb dating of detrital zircon from quartzite and magmatic zircon from a queluzite-hosted granodioritic dyke (Cabral *et al.*, 2019).

Queluzite orebodies are spatially associated with graphitic schist, quartz–biotite schist, garnet–amphibole schist, quartzite and amphibolite (see Fig. 1 of Cabral *et al.*, 2019). The latter consists mostly of hornblende with quartz, plagioclase and garnet, which originated from regional metamorphism of basaltic rocks (Herz & Banerjee, 1973). Amphibolitic rocks are interspersed with queluzite and graphitic schist, which were manganese-rich and manganese-poor carbonaceous muds, respectively. Their depositional setting, reconstructed by molybdenum isotopes, was an oxic–euxinic-stratified basin (Cabral *et al.*, 2019). At Morro da Mina, the rock succession hosting queluzite orebodies is isoclinally folded and sheared along ductile zones. Such shear zones are marked by graphitic schist and enclose sigmoidal orebodies of queluzite, which attain a maximum of 100 m in thickness. Queluzite orebodies are cut by granodioritic dykes (Hussak, 1906; Pires, 1983), the thermal effect of which may locally have exceeded the metamorphic temperature constrained by the assemblage rhodochrosite–tephroite–pyroxmangite, which indicates at least 600 °C (Peters *et al.*, 1974). Better temperature constraints and pressure–temperature–time paths are currently not available.

3. Sample material and methods

Queluzite samples were collected from the ore pile of the Morro da Mina mine. Polished sections were prepared for reflected-light microscopy and electron-microprobe analysis. Reconnaissance energy-dispersive spectroscopy (EDS) indicated Mn, Fe and S as major alabandite components with no other minor element.

Two electron microprobes were used, both operated in the wavelength-dispersive mode: a Cameca SX100 instrument, Technische Universität Clausthal (TUC), Germany; and a JEOL JXA-8230 instrument, Microscopy and Microanalysis Laboratory (LMic), Universidade Federal de Ouro Preto (UFOP), Brazil. Analytical conditions and X-ray lines used at the TUC were (reference materials in parentheses): 15 kV and 20 nA, beam size of 1 μm, and *K*α for S, Fe ($CuFeS_2$) and Mn (metallic Mn). Those implemented at the UFOP were 20 kV and 20 nA, and beam size of 1 μm. In order to check previous EDS work, measurements for other elements were carried out at the UFOP, the X-ray lines of which were: *L*α for As, Se and Mo (calibrated on InAs, and pure metals of Se and Mo, respectively); and *K*α for S, Mn, Fe, Co, Ni and Cu (calibrated on pure metals except for S and Fe, which had pyrite and magnetite, respectively, as reference materials). Both instruments had counting times of 10 s at peak position and 5 s at background position.

Silicate minerals were probed using the JEOL instrument at 15 kV and 20 nA, and beam size of 1 μm. Elements analysed for (*K*α lines) and their reference materials were: Si (quartz), Al (gahnite), Ti (rutile), Ca (fluor-apatite), Mg (olivine), Fe (almandine) and Mn (pure metal).

Aggregates with metallic lustre were hand-picked for X-ray diffraction. The concentrate was gently pulverised using an agate mortar with acetone. The powder, mounted on the surface of a low-background specimen holder, was measured on a Bruker D8 Advance diffractometer in the Bragg–Brentano geometry, with Cu*K*α radiation and Lynx Eye-XE detector, at the Czech Geological Survey, Prague. The diffraction data were collected in the angular range 4–80 °2θ with 0.015° steps at 1 s per step. Phase identification was carried out by means of the HighScore program (PANalytical, 2011).

4. Results

Alabandite occurs as patches in the interstices of the manganese-silicate and manganese-carbonate minerals that make up queluzite. The mineral forms either independent aggregates or composite aggregates with pyrrhotite and chalcopyrite (Fig. 2A). Patchy alabandite exhibits extensions that protrude into the queluzite matrix, along grain boundaries that are rectilinear and curvilinear, without fracturing the matrix minerals (Fig. 2A and B). Graphite, which is disseminated as flakes in the matrix, is commonly found as inclusions in alabandite (Fig. 2B). Chemically, alabandite does not show any obvious zoning with respect to either sulfur or manganese within individual grains (Fig. 2C and D). Chemical zoning is nevertheless recorded in alabandite-hosted molybdenite (Fig. 2E), which is locally rich in tungsten (Fig. 2F). Molybdenite is mostly observed as sandwich-like intergrowths with: (i) alabandite-hosted graphite (Fig. 2B); (ii) queluzite-disseminated graphite. The Morro da Mina alabandite has appreciable contents of iron, which vary from 5 to 13 mol% FeS (Table 1). The mean

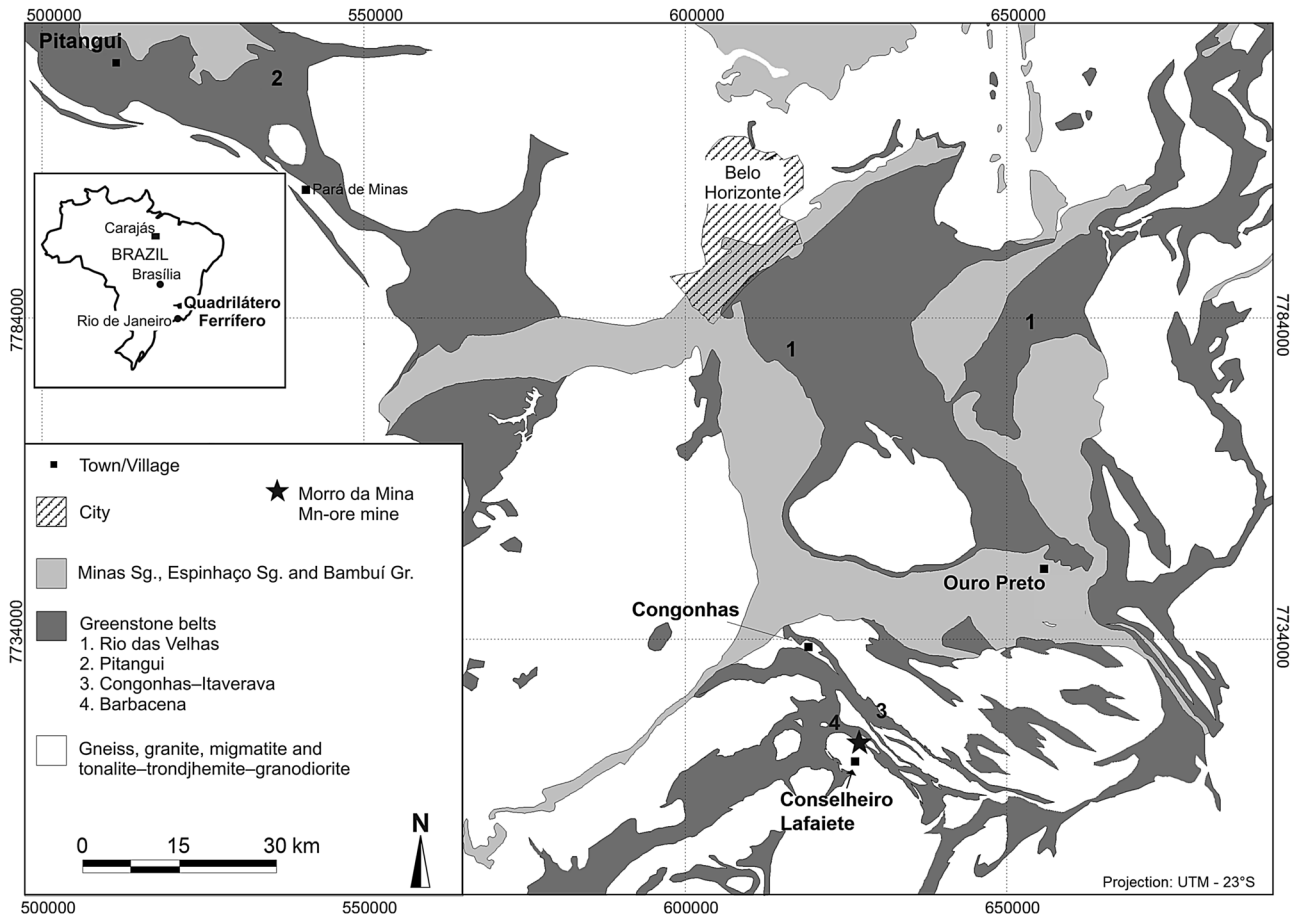

Fig. 1. Location of the Morro da Mina manganese-ore mine and distribution of greenstone belts in the Quadrilátero Ferrífero and adjacent areas, as compiled from Dorr (1969) and Corrêa Neto *et al.* (2012). Sg., Supergroup; Gr., Group.

composition of alabandite is 92.7 ± 1.4 mol% MnS and 7.3 ± 1.4 mol% FeS.

Spessartine, tephroite and rhodochrosite are the main manganese minerals that are spatially associated with alabandite (Figs. 2B and 3). Rhodonite and pyroxmangite were not observed in our sample collection. The mineral spessartine has MnO contents between 37 and 40 wt%, which are equivalent to 85–88 mol% spessartine (Table 2). The MnO content of tephroite is about 54 wt%, followed by 7–9 wt% FeO and 4–6 wt% MgO. The mineral rhodochrosite contains considerable amounts of calcium, as indicated by reconnaissance EDS and X-ray diffraction (see below and Fig. 3). An accessory mineral is worthy of attention: a bismuth telluride, which occurs as prolate flecks along the contact between spessartine crystals, defining a triple-point contact with interstitial rhodochrosite, *i.e.*, bismuth telluride–spessartine–rhodochrosite (Fig. 2B).

The optical and compositional identification of MnS as alabandite is confirmed by Rietveld analysis of X-ray diffraction data from a mineral concentrate (Fig. 4). In the concentrate, alabandite accounts for about 6 wt%, showing refined unit-cell parameter $a = 5.2133(2)$ Å (for $Fm\bar{3}m$ space group). The concentrate also shows major peaks of calcium-bearing rhodochrosite. The presence of calcium shifted the unit-cell parameters of rhodochrosite, the calculation of which gave $a = 4.799$ Å and $c = 15.883$ Å. These values are closer to ankerite ($a = 4.816$ Å and $c = 15.99$ Å), as compared to rhodochrosite, which should have $a = 4.768$ Å and $c = 15.63$ Å. Other minerals identified by X-ray diffraction are spessartine, tephroite and graphite (Fig. 4). About 1 wt% molybdenite was indicated by Rietveld analysis.

5. Discussion

5.1. Formation conditions of alabandite

The incorporation of iron into the cubic structure of alabandite has been suggested to be dependent on temperature: the higher the temperature, the more iron incorporated (*e.g.*, Skinner & Luce, 1971), a relationship that could hold in natural alabandite (Ramdohr, 1957). Nevertheless, subsequent investigations of alabandite from different localities worldwide, from unmetamorphosed to high-temperature settings (*e.g.*, Fukuoka, 1981; Törnroos, 1982; Schrauder *et al.*, 1993; Hurai & Huraiová, 2011), have indicated that the iron content in alabandite is not only dependent on temperature, but also very likely on FeS activity. This interpretation is supported by the composition of Morro da Mina alabandite,

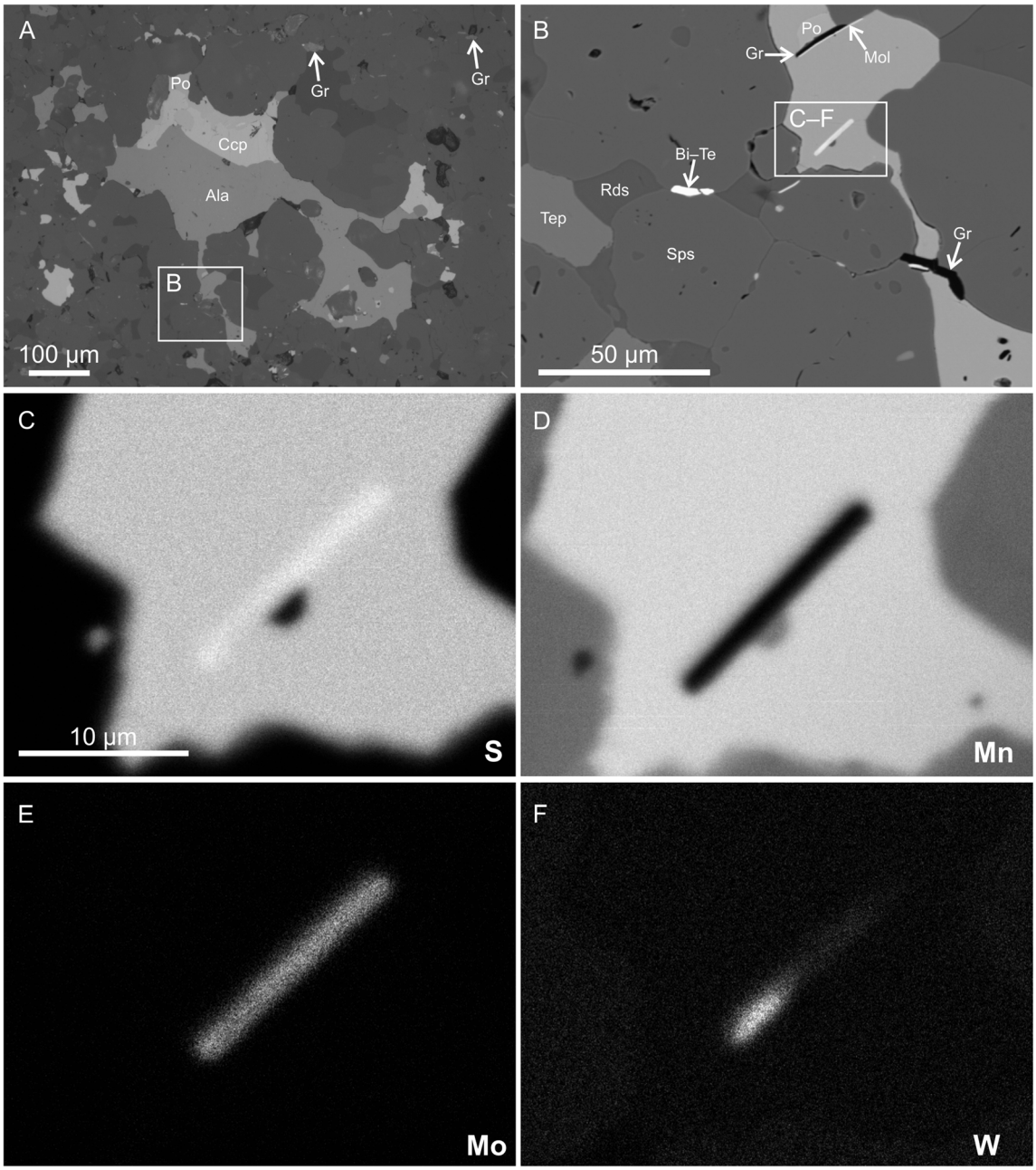

Fig. 2. (A) Reflected-light photomicrograph of alabandite (Ala) from Morro da Mina, Minas Gerais, Brazil. The mineral occurs as patches in the interstices of the carbonate–silicate matrix of queluzite, with and without chalcopyrite (Ccp) and pyrrhotite (Po). Graphite (Gr) is disseminated in the matrix. (B) Backscattered-electron image of the area delineated in (A), which shows that graphite is included in alabandite. Graphite is commonly intergrown with molybdenite (Mol), which is also found as independent crystals in alabandite. Spessartine (Sps), tephroite (Tep) and Ca-bearing rhodochrosite (Rds) are in the vicinity of alabandite, as well as a rarely observed bismuth telluride (Bi–Te). (C–F) Wavelength-dispersive X-ray maps for (C) sulfur, (D) manganese, (E) molybdenum and (F) tungsten of the area indicated in (B).

which has relatively low FeS contents overlapping those found in alabandite from unmetamorphosed bedded-type manganese deposits (Fig. 5; Fukuoka, 1981).

Could alabandite constrain the palaeoenvironmental conditions under which manganese-rich sediments precipitated? Schrauder *et al.* (1993) argued that alabandite in graphitic gneissic rocks containing manganese carbonate would be of metamorphic origin because sedimentary MnS would imply absence of CO_2 – *i.e.*, the presence of manganese carbonate would rule out the formation of sedimentary MnS. In contrast to that interpretation, assemblages of authigenic MnS and manganese carbonate have been described from modern anoxic marine sediments rich in organic matter (Suess, 1979; Böttcher & Huckriede, 1997; Lepland & Stevens, 1998). In the case of Morro da Mina, alabandite occupies interstitial spaces in the recrystallised matrix grains, which show triple contacts at approximately 120° (Fig. 2B). Such contacts suggest that the Morro da Mina

Table 1. Electron-microprobe analyses of alabandite from Morro da Mina, Minas Gerais, Brazil.

	Mn	Fe	S	Total	Mn	Fe	S	MnS	FeS
Spot no.	wt%	wt%	wt%	wt%	*apfu*	*apfu*	*apfu*	mol%	mol%
1	57.96	4.20	37.22	99.38	0.92	0.07	1.01	93.4	6.6
2*	57.86	4.09	37.49	99.44	0.92	0.06	1.02	93.5	6.5
3	57.63	4.57	37.37	99.57	0.91	0.07	1.02	92.8	7.2
4	57.71	4.56	37.35	99.61	0.91	0.07	1.01	92.8	7.2
5	58.19	4.07	36.96	99.21	0.93	0.06	1.01	93.6	6.4
6	58.05	3.78	37.76	99.60	0.92	0.06	1.02	94.0	6.0
7*	57.88	4.52	37.09	99.48	0.92	0.07	1.01	92.9	7.1
8	59.16	3.17	37.20	99.53	0.94	0.05	1.01	95.0	5.0
9	58.18	3.79	37.21	99.18	0.93	0.06	1.01	94.0	6.0
10	58.48	3.56	37.11	99.15	0.93	0.06	1.01	94.4	5.6
11	57.77	4.45	36.88	99.10	0.92	0.07	1.01	92.9	7.1
12	57.66	4.03	37.36	99.05	0.92	0.06	1.02	93.6	6.4
13	58.57	3.75	37.16	99.48	0.93	0.06	1.01	94.1	5.9
14	57.44	5.17	36.78	99.39	0.91	0.08	1.00	91.9	8.1
15	57.70	5.59	36.55	99.84	0.92	0.09	1.00	91.3	8.7
16	57.53	5.49	36.52	99.54	0.92	0.09	1.00	91.4	8.6
17	58.13	5.29	36.39	99.81	0.92	0.08	0.99	91.8	8.2
18	58.07	4.79	36.74	99.60	0.92	0.07	1.00	92.5	7.5
19	58.34	4.85	37.06	100.25	0.92	0.08	1.00	92.4	7.6
20	57.34	5.62	36.55	99.51	0.91	0.09	1.00	91.2	8.8
21	59.10	4.43	36.93	100.46	0.93	0.07	1.00	93.1	6.9
22	55.21	8.43	36.64	100.28	0.87	0.13	0.99	86.9	13.1
23	58.82	4.10	36.51	99.43	0.94	0.06	1.00	93.6	6.4
24	58.95	4.32	36.67	99.94	0.94	0.07	1.00	93.3	6.7
25	58.56	4.44	36.66	99.66	0.93	0.07	1.00	93.1	6.9
26	58.63	4.29	36.69	99.61	0.93	0.07	1.00	93.3	6.7
27	58.43	4.57	37.19	100.19	0.92	0.07	1.01	92.9	7.1
28	58.85	4.07	36.61	99.53	0.94	0.06	1.00	93.6	6.4
29	58.22	4.82	36.87	99.91	0.92	0.08	1.00	92.5	7.5
30	59.80	3.67	36.84	100.31	0.94	0.06	1.00	94.3	5.7
31	57.67	5.57	37.23	100.47	0.91	0.09	1.01	91.3	8.7
32	56.95	6.17	36.67	99.79	0.90	0.10	1.00	90.4	9.6
33	59.75	3.43	36.49	99.67	0.95	0.05	1.00	94.7	5.3
34	57.21	5.40	36.46	99.07	0.92	0.08	1.00	91.5	8.5
35	58.49	4.89	36.85	100.23	0.92	0.08	1.00	92.4	7.6
36	57.89	5.16	36.75	99.80	0.92	0.08	1.00	91.9	8.1
37	58.52	4.67	36.68	99.87	0.93	0.07	1.00	92.7	7.3
38	58.19	4.75	36.30	99.24	0.93	0.07	0.99	92.6	7.4

*Spots 2 and 7 have 0.08 and 0.07 wt% Se, respectively. Atoms per formula unit (*apfu*) on the basis of two atoms. Spots 1–13 and 14–38 were measured using a JEOL instrument (UFOP, Ouro Preto, Brazil) and a Cameca instrument (TUC, Clausthal, Germany), respectively – see Section 3. Spots 1–13 were additionally measured for the following metals, the contents of which were below the detection limit (in parenthesis, wt%): Co (0.04); Ni (0.08); Cu (0.10); As (0.10); Se (0.06); Mo (0.10).

alabandite either crystallised or recrystallised during metamorphism and did not react to form the matrix minerals. It is likely that the alabandite crystals had an authigenic origin as MnS in a carbon- and sulfur-rich anoxic sedimentary rock, such as carbonaceous marl. Such an origin is consistent with the widespread dissemination of graphite in queluzite and the spatial association of alabandite with graphite and molybdenite, which in places shows a high tungsten-sulfide component of up to 20 mol% WS_2 (Cabral *et al.*, 2017). The latter minerals and solid solutions indicate that the manganese authigenesis at Morro da Mina was not only anoxic, but also highly sulfidic.

Alabandite stability covers the fields of iron, pyrrhotite and pyrite (Fig. 6A), under conditions that are invariably reduced. Hauerite (MnS_2) forms only at extreme sulfur fugacity close to sulfur condensation, whereas the alabandite stability field expands with increasing temperature (Holland, 1959). The latter is confirmed by currently available thermodynamic data, which are provided from 0 to 300 °C (Fig. 6B; Geochemists's Workbench): the oxygen fugacity at 300 °C in equilibrium with $MnSO_4$ is essentially 40 log units higher than that at 25 °C. At 600 °C, a minimum estimate for the metamorphic temperature at Morro da Mina (Peters *et al.*, 1974), the alabandite stability field expands to even higher oxygen fugacities.

At Morro da Mina, the coexistence of alabandite and pyrrhotite (Fig. 2A and B) points to a definitely anoxic environment. Anoxic environments become sulfidic, or euxinic, where the concentration of dissolved sulfide attains the threshold needed to form MnS. This threshold is suggested to be at $[H_2S] \geq 10^{-6}$ M (Berner, 1981), a concentration that is approximately three orders of magnitude lower than

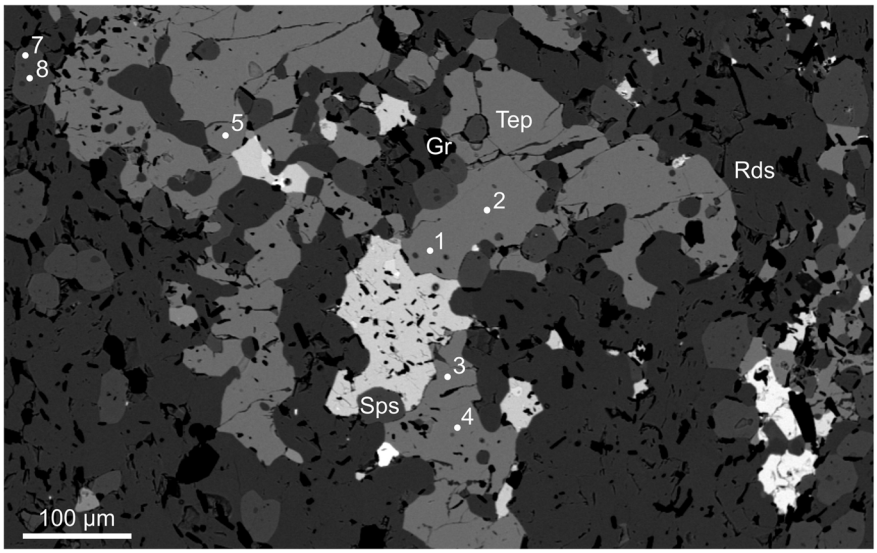

Fig. 3. Backscattered-electron image of alabandite aggregates (bright domains) in queluzite, a rock that consists of Ca-bearing rhodochrosite (Rds), spessartine (Sps), tephroite (Tep) and graphite (Gr). The alabandite aggregate at the centre has abundant inclusions of graphite (black). Numbers refer to spots of electron-microprobe analyses in Table 2. Two compositional types of carbonate coexist as individual grains in apparent equilibrium with spessartine and/or tephroite in this sample. Their approximate compositions are $(Mn_{0.70}Ca_{0.18}Mg_{0.11}Fe_{0.01})CO_3$ and $(Mn_{0.71}Ca_{0.02}Mg_{0.12}Fe_{0.16})CO_3$.

Table 2. Electron-microprobe analyses of tephroite and spessartine from Morro da Mina, Minas Gerais, Brazil.

Spot no.		1	2	3	4	5	7	8	9	10
SiO_2	wt%	31.57	31.97	31.13	30.63	32.73	36.40	36.80	36.75	37.59
Al_2O_3		<0.08	<0.08	<0.08	<0.08	<0.08	20.70	20.76	20.96	20.95
TiO_2		<0.03	<0.03	<0.03	<0.03	0.20	0.14	0.11	0.25	0.03
FeO		8.19	8.98	8.16	8.69	7.02	1.71	1.72	1.17	1.17
MnO		54.37	54.66	54.01	54.78	54.57	38.42	37.69	36.68	36.27
MgO		5.47	4.12	5.28	5.78	4.47	1.02	0.76	0.60	0.45
CaO		<0.04	<0.04	0.05	0.07	0.06	2.16	1.81	2.92	2.81
Total		99.60	99.72	98.63	99.95	99.05	100.54	99.65	99.34	99.25
Si	*apfu*	1.022	1.044	1.019	0.988	1.071	2.950	3.011	3.009	3.079
Al							1.977	2.002	2.022	2.022
Ti						0.005	0.008	0.007	0.016	0.002
Fe		0.222	0.245	0.223	0.235	0.192	0.116	0.118	0.080	0.080
Mn		1.491	1.511	1.498	1.497	1.512	2.638	2.611	2.544	2.516
Mg		0.264	0.200	0.258	0.278	0.218	0.187	0.158	0.256	0.247
Ca				0.002	0.002	0.002	0.124	0.092	0.074	0.055
Tep		75.4	77.2	75.6	74.4	78.6				
Fo		13.3	10.2	13.0	13.8	11.3				
Fa		11.2	12.5	11.3	11.7	10.0				
Sps	mol%						86.1	87.6	86.1	86.8
Alm							3.8	3.9	2.7	2.8
Pyr							4.0	3.1	2.5	1.9
Gro							5.6	4.9	7.6	8.4
Sch							0.6	0.5	1.0	0.1

Atoms per formula unit (*apfu*) on the basis of three cations for tephroite (spots 1–5) and eight cations for spessartine (spots 7–10). Abbreviations of end-member minerals: Tep, tephroite; Fo, forsterite; Fa, fayalite; Sps, spessartine; Alm, almandine; Pyr, pyrope; Gro, grossular; Sch, schorlomite.

that required to effectively scavenge thiomolybdate species from euxinic seawater by organic matter (Helz *et al.*, 1996). Scavenging of seawater molybdenum as thiomolybdate is enhanced by sulfur-rich organic matter (Tribovillard *et al.*, 2004), leading to the C/MoS_2 mixed-layer phase that, for example, occurs in weakly metamorphosed black shales of Early Cambrian age in southern China (Kao *et al.*, 2001). The molybdenite–graphite aggregates shown in Fig. 2B are likely the metamorphic equivalent under amphibolite-facies conditions of the C/MoS_2 mixed-layer phase found in black shales from euxinic basins (Cabral *et al.*, 2017).

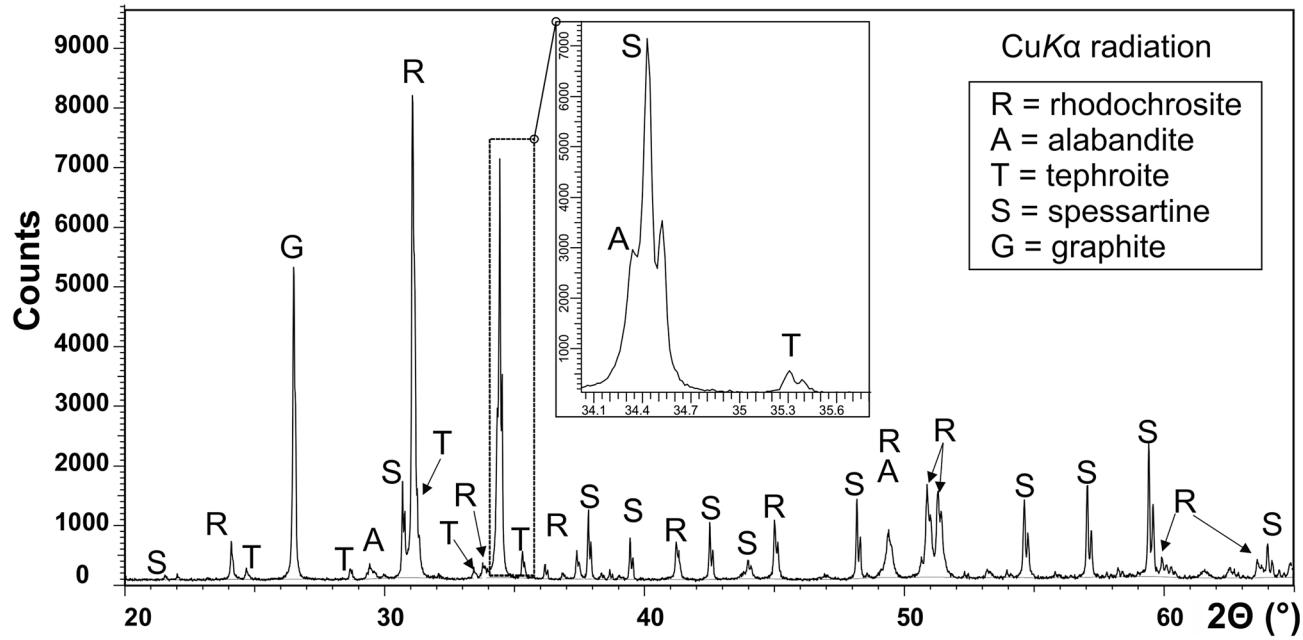

Fig. 4. X-ray powder diffraction pattern of a concentrate of aggregates with metallic lustre. Alabandite is identified in the inset.

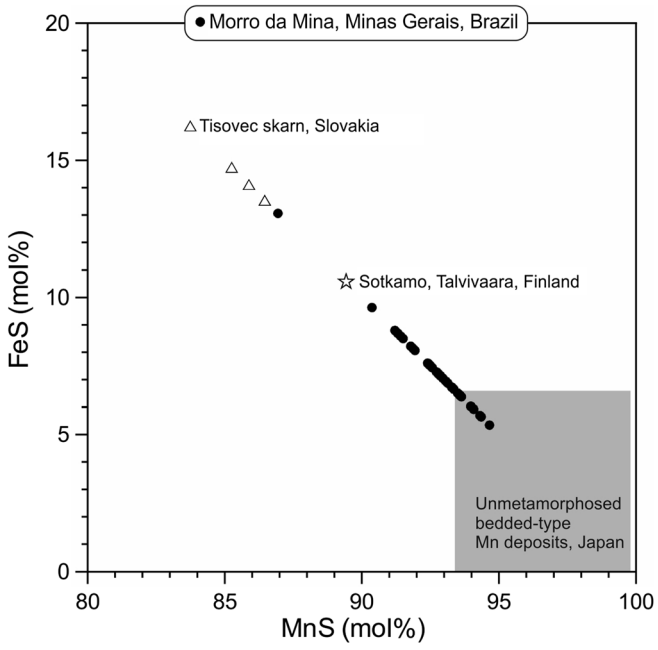

Fig. 5. Bivariate plot of MnS *vs.* FeS contents in alabandite from Morro da Mina, Minas Gerais, Brazil. For comparison, compositions of alabandite from some localities are plotted: the Tisovec skarn, Slovakia (Hurai & Huraiová, 2011); the metamorphosed black-shale-hosted Talvivaara deposit, Finland (Törnroos, 1982); unmetamorphosed bedded-type manganese deposits, Japan (Fukuoka, 1981).

The euxinic, sulfidic character of manganese sedimentation at Morro da Mina is additionally supported by the occurrence of tungsten-bearing molybdenite (Fig. 2F), as the geochemical switch of seawater-conservative tungstate to particle-reactive thiotungstate requires dissolved sulfide concentrations that are even higher (~3 orders of magnitude) than those needed for thiomolybdate formation (Mohajerin *et al.*, 2016).

5.2. Alabandite assemblages as palaeonvironmental indicators

A compilation of alabandite occurrences worldwide indicates that alabandite not only occurs together with graphite and molybdenite, as found at Morro da Mina, but also in a variety of mineral assemblages. It is thus likely that alabandite-bearing mineral assemblages in metasedimentary deposits reflect different environmental conditions. In general, four assemblages can be distinguished:

1. alabandite + graphite;
2. alabandite + graphite + molybdenite;
3. alabandite + rhodochrosite + molybdenite; and
4. alabandite + rhodochrosite.

Assemblage (1) is represented by graphitic gneissic rocks in the Moldanubian zone of the Bohemian massif, Austria (Schrauder *et al.*, 1993). Their precursory sediments were deposited at <550 Ma, and underwent a high-grade metamorphic overprint during the Variscan orogeny at *ca.* 340 Ma. The graphite–alabandite assemblage suggests that organic-matter scavenging of thiomolybdate species from seawater did not occur, as molybdenite is missing in those rocks. Their contents of redox-sensitive elements, such as molybdenum and nickel, are not substantially enriched in relation to the upper continental crust (see Schrauder *et al.*, 1993). It can therefore be proposed that MnS originally precipitated from pore waters within ocean-floor sediments during diagenesis, and that the seawater column was not euxinic.

Assemblage (2) occurs at Morro da Mina (Fig. 2), as well as in manganese-rich graphitic schist and metacarbonate

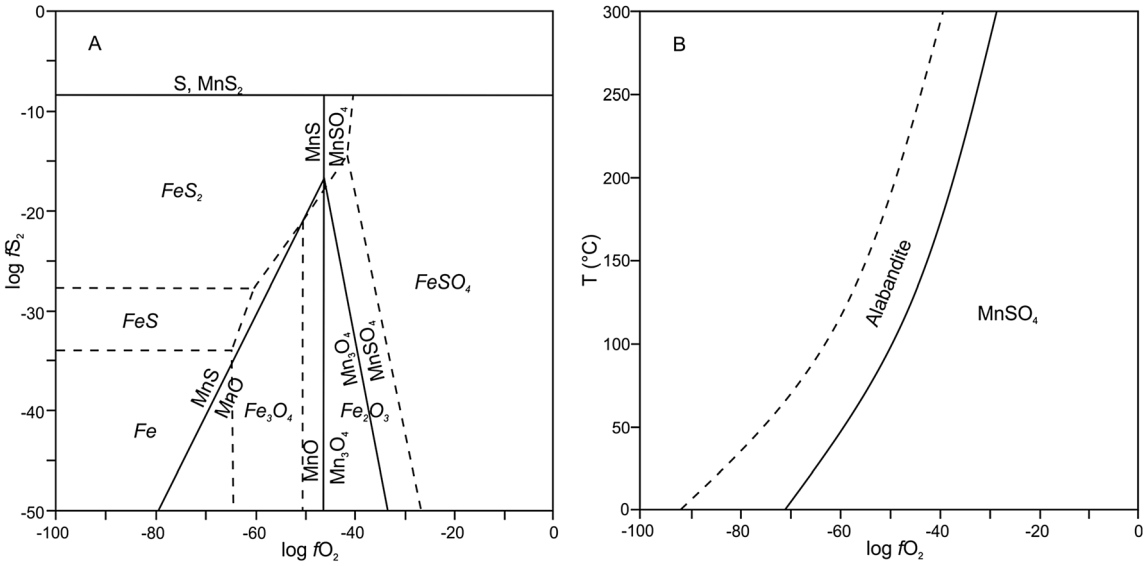

Fig. 6. (A) Diagram of oxygen fugacity (fO_2) *vs.* sulfur fugacity (fS_2) at 1 atm showing the superposition of stability fields of iron minerals (dashed lines) and manganese minerals at 400 K, according to Holland (1959). The coexistence of alabandite and pyrrhotite at Morro da Mina indicates reduced conditions. (B) Diagram of oxygen fugacity (fO_2) *vs.* temperature, calculated using Geochemist's Workbench (at 1 atm pressure below 100 °C and along the vapour pressure at higher temperatures, and activities for alabandite and water at 0.001 and 1, respectively). Dashed line shows stability limits for water at 1 atm pressure.

rocks at Talvivaara, Finland (Loukola-Ruskeeniemi & Lahtinen, 2013; Kontinen & Hanski, 2015). Those rocks were deposited 2.1–1.9 Ga ago, and underwent amphibolite-facies metamorphism. Loukola-Ruskeeniemi & Lahtinen (2013) laconically mentioned that "molybdenite occurs associated with graphite flakes", a description that is suggestive of graphite–molybdenite aggregates. The assemblage alabandite–graphite–molybdenite points to a euxinic setting, a conclusion that is supported by the enrichment of redox-sensitive elements. One of these diagnostic elements is nickel, which is enriched at both Talvivaara and Morro da Mina in the 1000 ppm range. It is interesting to mention that the best age constraint for Morro da Mina – *i.e.*, 2.07–1.86 Ga – indicates that the queluzite-precursory sediments were coeval with those at Talvivaara. Indeed, the period between 2.1 and 1.9 Ga was marked by worldwide deposition of carbonaceous sediments, some of which led to black-shale-hosted manganese deposits (Roy, 1992; Condie *et al.*, 2001).

Assemblage (3) is reported from the Nsuta manganese deposit in the Ashanti belt of southern Ghana (Mücke *et al.*, 1999). Manganese-rich sediments at Nsuta accumulated during the Birimian at *ca.* 2.17 Ga, and experienced a greenschist-facies metamorphic overprint during the Eburnian period at ~2.1 Ga. At Nsuta, graphite is absent, but alabandite and molybdenite are in the vicinity of each other in a matrix of rhodochrosite (Plate 1A of Mücke *et al.*, 1999). Rhodochrosite carbon was sourced from organic matter (Yeh *et al.*, 1995). However, there is no petrographical evidence that connects molybdenite with organic matter, neither in the form of graphite nor carbonaceous material, making it unlikely that molybdenite originated from organic-matter scavenging of thiomolybdate species from euxinic seawater. Instead, the association of molybdenum with authigenic manganese carbonate would rather suggest that the molybdenum had been released from manganese-oxide sediments during reductive diagenesis (Shimmield & Price, 1986; Shaw *et al.*, 1990).

Assemblage (4) is exemplified by the Tiantaishan phosphorite–manganese-carbonate deposit of Early Cambrian age in southern Shaanxi province of China (Hein *et al.*, 1999). Its sedimentary rocks are weakly metamorphosed. Alabandite is restricted to the rhodochrosite-ore section, which has low contents of total organic carbon, molybdenum and nickel. Such characteristics indicate that manganese deposition took place as oxide in low-oxygen bottom waters – *i.e.*, dysoxic zone. Following burial, manganese-oxide sediments gave rise to rhodochrosite and alabandite, for which carbon and sulfur were provided from the oxidation of organic matter and bacterial sulfate reduction (Okita *et al.*, 1988; Hein *et al.*, 1999).

Other occurrences of alabandite with and without rhodochrosite, in which molybdenite and graphite have not been reported, are known from chert-hosted manganese deposits in the accretionary complexes of the Japanese Islands (Nakagawa *et al.*, 2009, 2011). Alabandite is found in mineral assemblages containing manganese-bearing pyroxene and amphibole, which record the metamorphic overprint by Cretaceous granitic intrusions. In the absence of graphite and/or molybdenite, it is difficult to interpret the palaeoenvironmental significance of alabandite in such assemblages. The mineral could reflect: (i) locally reducing conditions that were induced by contact metamorphism; or (ii) within-sediment reductive dissolution of manganese-oxide precipitates in the presence of sulfidic pore water [*cf.* Assemblages (3) and (4)]. The second hypothesis is favoured on the basis of sulfur-isotope data that are indicative of bacterial sulfate reduction (Sasaki *et al.*, 1985;

Komuro *et al.*, 2005). Interestingly, the chert-hosted manganese deposits have been considered manganese-oxide siliceous sediments of the ocean floor that were metamorphosed during the subduction–accretion process (Nakagawa *et al.*, 2009, 2011).

Despite all uncertainties that are inherent in reflected-light microscopy, the point to be stressed here is the recognition of graphite, molybdenite and alabandite. This mineral assemblage very likely fingerprints a euxinic water column in a stratified ocean, where seawater molybdenum was scavenged by sulfurised organic matter beneath the oxic–euxinic chemocline. Such carbonaceous sediments are enriched in nickel. Metamorphic overprint on manganese-rich sediments containing sulfurised organic matter resulted in a close spatial association of graphite, molybdenite and alabandite (Fig. 2). Alabandite without graphite–molybdenite aggregates probably precipitated from sulfidic pore waters in sea-floor sediments, primarily deposited under oxic or anoxic bottom waters.

6. Conclusion

The Morro da Mina alabandite has some iron in solid solution, the mean content of which is 7.3 ± 1.4 mol% FeS. The mineral is spatially associated with graphite–molybdenite aggregates. Using a reflected-light microscope, a first-step approach to decipher palaeoenvironmental conditions of metasedimentary manganese-bearing rocks is the recognition of the following assemblages: (1) alabandite + graphite; (2) alabandite + graphite + molybdenite; (3) alabandite + rhodochrosite + molybdenite; and (4) alabandite + rhodochrosite. Among them, only the second assemblage fingerprints molybdenum scavenging by organic matter in euxinic seawater in a stratified ocean. The molybdenite of assemblage (3) results from the diagenetic reduction of manganese-oxide sediments, which released their adsorbed molybdenum to sulfidic pore waters.

Acknowledgements: We acknowledge the Microscopy and Microanalysis Laboratory (LMic) of the Universidade Federal de Ouro Preto, a member of the FAPEMIG-supported Microscopy and Microanalysis Network of Minas Gerais. The Brazilian Research Council (CNPq) is thanked for granting a fellowship to G. Queiroga. Two anonymous reviewers contributed to improve the manuscript and are gratefully acknowledged, as well as the editorial handling by C. Rodriguez-Navarro and an Associate Editor. C. Chopin is thanked for his attentive reading of the accepted manuscript.

References

Baron, G. & Debyser, J. (1957): Sur la présence dans des vases organiques de la mer Baltique du sulfure manganeux β–hexagonal. *C. R. Acad. Sci.*, **245**, 1148–1150.

Berner, R.A. (1981): A new geochemical classification of sedimentary environments. *J. Sedim. Petrol.*, **51**, 359–365.

Böttcher, M.E. & Huckriede, H. (1997): First occurrence and stable isotope composition of authigenic γ-MnS in the central Gotland Deep (Baltic Sea). *Mar. Geol.*, **137**, 201–205.

Cabral, A.R., Zeh, A., Viana, N.C. da S., Schirmer, T., Lehmann, B. (2017): Graphite–$(Mo,W)S_2$ intergrowth as a palaeoenvironmental proxy in metasedimentary rocks. *Lithos*, **294–295**, 412–417.

Cabral, A.R., Zeh, A., Viana, N.C., Ackerman, L., Pašava, J., Lehmann, B., Chrastný, V. (2019): Molybdenum-isotope signals and cerium anomalies in Palaeoproterozoic manganese ore survive high-grade metamorphism. *Sci. Rep.*, **9**, 4570 (www.nature.com/articles/s41598-019-40998-5).

Candia, M.A.F. & Girardi, V.A.V. (1979): Aspectos metamórficos da Formação Lafaiete em Morro da Mina, distrito de Lafaiete, MG. *Bol. IG (Inst. Geociênc., USP)*, **10**, 19–30.

Condie, K.C., Des Marais, D.J., Abbott, D. (2001): Precambrian superplumes and supercontinents: a record in black shales, carbon isotopes, and paleoclimates? *Precambr. Res.*, **106**, 239–260.

Corrêa Neto, A.V., de Modesto, A.M., Caputo Neto, V., Guerrero, J.C. (2012): Alteração hidrotermal em zona de cisalhamento associada ao Lineamento Congonhas, sul do Quadrilátero Ferrífero, Minas Gerais. *Anu. Inst. Geociênc. (UFRJ)*, **35**, 55–64.

Dasgupta, S., Banerjee, H., Fukuoka, M., Bhattacharya, P.K., Roy, S. (1990): Petrogenesis of metamorphosed manganese deposits and the nature of the precursor sediments. *Ore Geol. Rev.*, **5**, 359–384.

Derby, O.A. (1901): On the manganese ore deposits of the Queluz (Lafayette) district, Minas Geraes, Brazil. *Am. J. Sci.*, **12**, 18–32.

— (1908): On the original type of the manganese ore deposits of the Queluz district, Minas Geraes, Brazil. *Am. J. Sci.*, **25**, 213–216.

Dorr , J.V.N. (1969): Physiographic, stratigraphic and structural development of the Quadrilátero Ferrífero, Minas Gerais, Brazil. *U. S. Geol. Surv. Prof. Paper*, **641-A**, 110.

Ebert, H. (1957): Beitrag zur Gliederung des Präkambriums in Minas Gerais. *Geol. Rundsch.*, **45**, 471–521.

— (1962): Baustil und Regionalmetamorphose im präkambrischen Grundgebirge Brasiliens. *Tschermaks Mineral. Petrogr. Mitt.*, **8**, 49–81.

Fukuoka, M. (1981): Mineralogical and genetical study on alabandite from manganese deposits of Japan. *Mem. Fac. Sci. Kyushu Univ. D*, **24**, 207–251.

Grossi Sad, J.H., Pinto, C.P., Duarte, C.L. (1983): Geologia do distrito manganesífero de Conselheiro Lafaiete, MG. *Bol. – Núcleo Minas Gerais Soc. Bras. Geol.*, **3**, 259–270.

Guimarães, D. (1929): Sobre a genese dos minerios de manganez do districto de Lafayette. *An. Acad. Bras. Sci.*, **1**, 179–182.

Gutzmer, J. & Beukes, N.J. (2009): Iron and manganese ore deposits: mineralogy, geochemistry, and economic geology. *in* "Encyclopedia of life support systems – geology, volume IV", B. De Vivo, B. Grasemann, K. Stüwe, eds. UNESCO, Eolss Publishers, Oxford, 43–69.

Hein, J.R., Fan, D., Ye, J., Liu, T., Yeh, H.-W. (1999): Composition and origin of Early Cambrian Tiantaishan phosphorite–Mn carbonate ores, Shaanxi Province, China. *Ore Geol. Rev.*, **15**, 95–134.

Helz, G.R., Miller, C.V., Charnock, J.M., Mosselmans, J.F.W., Pattrick, R.A.D., Garner, C.D., Vaughan, D.J. (1996): Mechanism of molybdenum removal from the sea and its concentration in black shales: EXAFS evidence. *Geochim. Cosmochim. Acta*, **60**, 3631–3642.

Herz, N. & Banerjee, S. (1973): Amphibolites of the Lafaiete, Minas Gerais, and the Serra do Navio manganese deposits, Brazil. *Econ. Geol.*, **68**, 1289–1296.

Holland, H.D. (1959): Some applications of thermochemical data to problems of ore deposits. I. Stability relations among the oxides, sulfides, sulfates and carbonates of ore and gangue metals. *Econ. Geol.*, **54**, 184–233.

Hurai, V. & Huraiová, M. (2011): Origin of ferroan alabandite and manganoan sphalerite from the Tisovec skarn, Slovakia. *N. Jb. Mineral. Abh.*, **188**, 119–134.

Hussak, E. (1906): Über die Manganerzlager Brasiliens. *Z. Prakt. Geol.*, **14**, 237–239.

Jinglan, L. (1987): Gold deposits in Precambrian banded iron-formations – a case study of the Dongfengshan gold deposit. *Acta Geol. Sin.*, **61**, 67–82.

Kao, L.-S., Peacor, D.R., Coveney, R.M., Zhao, G., Dungey, K.E., Curtis, M.D., Penner-Hahn, J.E. (2001): A C/MoS_2 mixed-layer phase (MoSC) occurring in metalliferous black shales from southern China, and new data on jordisite. *Am. Mineral.*, **86**, 852–861.

Komuro, K., Yamaguchi, K., Kajiwara, Y. (2005): Chemistry and sulfur isotopes in a chert-dominant sequence around the stratiform manganese deposit of the Noda-Tamagawa mine, northern Kitakami Terrane, northeast Japan: implication for Paleoceanographic environmental setting. *Res. Geol.*, **55**, 337–351.

A. Kontinen & E. Hanski (2015): The Talvivaara black-shale-hosted Ni–Zn–Cu–Co deposit in eastern Finland. *in* "Mineral deposits of Finland", W.D. Maier, R. Lahtinen, H. O'Brien, eds. Elsevier, Amsterdam, The Netherlands, 557–612.

Lepland, A. & Stevens, R.L. (1998): Manganese authigenesis in the Landsort Deep, Baltic Sea. *Mar. Geol.*, **151**, 1–25.

Loukola-Ruskeeniemi, K. & Lahtinen, H. (2013): Multiphase evolution in the black-shale-hosted Ni–Cu–Zn–Co deposit at Talvivaara, Finland. *Ore Geol. Rev.*, **52**, 85–99.

Miller, B.L. & Singewald, J.T. (1917): The manganese ores of the Lafayette district, Minas Geraes, Brazil. *Trans. Am. Inst. Min. Eng.*, **56**, 7–30.

Mohajerin, T.J., Helz, G.R., Johannesson, K.H. (2016): Tungsten–molybdenum fractionation in estuarine environments. *Geochim. Cosmochim. Acta*, **177**, 105–119.

Mücke, A., Dzigbodi-Adjimah, K., Annor, A. (1999): Mineralogy, petrography, geochemistry and genesis of the Paleoproterozoic Birimian manganese-formation of Nsuta/Ghana. *Mineral. Deposita*, **34**, 297–311.

Nakagawa, M., Santosh, M., Maruyama, S. (2009): Distribution and mineral assemblages of bedded manganese deposits in Shikoku, Southwest Japan: implications for accretion tectonics. *Gondw. Res.*, **16**, 609–621.

—, —, — (2011): Manganese formations in the accretionary belts of Japan: implications for subduction–accretion process in an active convergent margin. *J. Asian Earth Sci.*, **42**, 208–222.

Noce, C.M., Teixeira, W., Quéméneur, J.J.G., Martins, V.T.S., Bolzachini, E. (2000): Isotopic signatures of Paleoproterozoic granitoids from the southern São Francisco craton and implications for the evolution of the Transamazonian orogeny. *J. South Am. Earth Sci.*, **13**, 225–239.

Okita, P.M., Maynard, J.B., Spiker, E.C., Force, E.R. (1988): Isotopic evidence for organic matter oxidation by manganese reduction in the formation of stratiform manganese carbonate ore. *Geochim. Cosmochim. Acta*, **52**, 2679–2685.

PANalytical, B.V. (2011): HighScore 3.0. Almelo, The Netherlands.

Park, C.F. , Dorr , J.V.N., Guild, P.W., Barbosa, A.L.M. (1951): Notes on the manganese ores of Brazil. *Econ. Geol.*, **46**, 1–22.

Peters, T., Valarelli, J.V., Candia, M.A. (1974): Petrogenetic grids from experimental data in the system Mn–Si–C–O–H. *Rev. Bras. Geoci.*, **4**, 15–26.

Pires, F.R.M. (1978): The Archaean Barbacena greenstone belt in its typical development and the Minas itabirite distribution at the Lafaiete district, Minas Gerais. *An. Acad. Bras. Ciênc.*, **50**, 599–600.

— (1983): Manganese mineral parageneses at the Lafaiete district, Minas Gerais, Brazil. *An. Acad. Bras. Ciênc.*, **55**, 271–285.

Ramdohr, P. (1957): Eisenalabandin, ein merkwürdiger natürlicher Hochtemperatur-Mischkristall. *N. Jb. Mineral. Abh.*, **91**, 89–93.

Roy, S. (1965): Comparative study of the metamorphosed manganese protores of the world – the problem of the nomenclature of the gondites and kodurites. *Econ. Geol.*, **60**, 1238–1260.

— (1992): Environments and processes of manganese deposition. *Econ. Geol.*, **87**, 1218–1236.

Roy, S. & Purkait, P.K. (1968): Mineralogy and genesis of the metamorphosed manganese silicate rocks (gondite) of Gowari Wadhona, Madhya Pradesh, India. *Contrib. Mineral. Petrol.*, **20**, 86–114.

Sasaki, A., Hirowatari, F., Fukuoka, M. (1985): A sulfur isotopic study of alabandites from some manganese ore deposits in Japan. *Mineral. Geol.*, **35**, 51–56.

Schrauder, M., Beran, A., Hoernes, S., Richter, W. (1993): Constraints on the origin and the genesis of graphite-bearing rocks from the Variegated Sequence of the Bohemian massif (Austria). *Mineral. Petrol.*, **49**, 175–188.

Shaw, T.J., Gieskes, J.M., Jahnke, R.A. (1990): Early diagenesis in differing depositional environments: the response of transition metals in pore water. *Geochim. Cosmochim. Acta*, **54**, 1233–1246.

Shimmield, G.B. & Price, N.B. (1986): The behavior of molybdenum and manganese during early sediment diagenesis – offshore Baja California, Mexico. *Mar. Chem.*, **19**, 261–280.

Skinner, B.J. & Luce, F.D. (1971): Solid solutions of the type (Ca, Mg, Mn, Fe)S and their use as geothermometers for the enstatite chondrites. *Am. Mineral.*, **56**, 1269–1296.

Suess, E. (1979): Mineral phases formed in anoxic sediments by microbial decomposition of organic matter. *Geochim. Cosmochim. Acta*, **43**, 339–352.

Törnroos, R. (1982): Properties of alabandite; alabandite from Finland. *N. Jb. Mineral. Abh.*, **144**, 107–123.

Tribovillard, N., Riboulleau, A., Lyons, T., Baudin, F. (2004): Enhanced trapping of molybdenum by sulfurized marine organic matter of marine origin in Mesozoic limestones and shales. *Chem. Geol.*, **213**, 385–401.

Viana, N.C. da S. (2009): Mineralogia, calcinação e nova classificação tipológica de minérios de manganês sílico-carbonatados. M.Sc. thesis. Universidade Federal de Ouro Preto, Ouro Preto, Brazil, http://www.repositorio.ufop.br/handle/123456789/3086.

Yeh, H.-W., Hein, J.R., Bolton, B.R. (1995): Origin of the Nsuta manganese carbonate proto-ore, Ghana: carbon- and oxygen-isotope evidence. *J. Geol. Soc. China*, **38**, 397–409.

Received 6 December 2018
Modified version received 4 April 2019
Accepted 12 April 2019